第130巻　第 3 号　2022年 3 月 1 日発行（毎月1回1日発行）　ISSN 1348-6535 CODEN: JCSJEW

JCS-Japan

March

vol.130

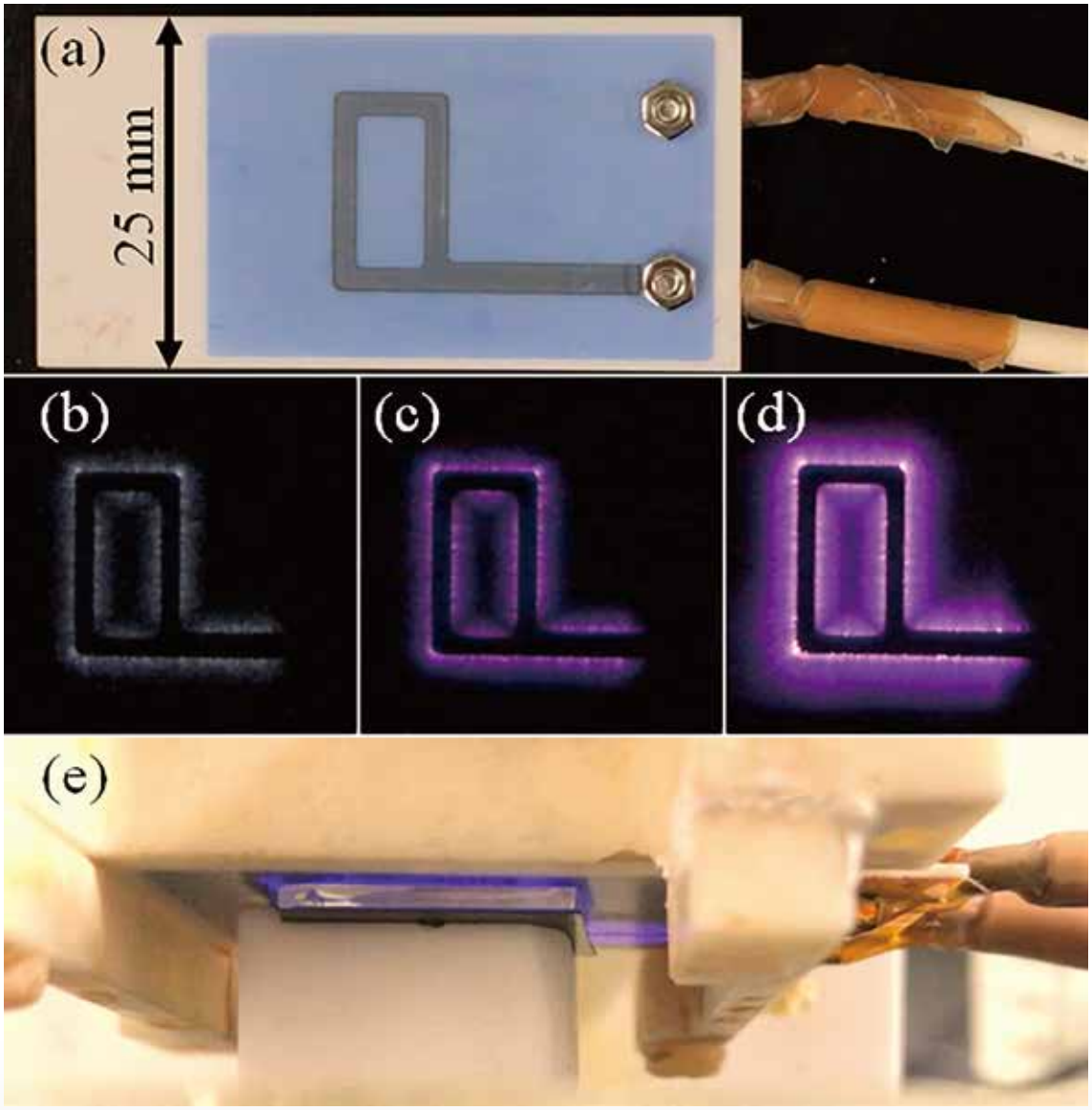

Journal of the Ceramic Society of Japan

2022

Journal of the Ceramic Society of Japan 130 [3] 249-256 2022
DOI http://doi.org/10.2109/jcersj2.21160

JCS-Japan

FULL PAPER

Atmospheric non-equilibrium planar plasma under magnetic field to form a porous-TiO_2 layer for dye-sensitized solar cells

Yuki Nagao[1], Shinji Mayumi[1], Minato Sawamura[1], Ryosuke Okumura[1] and Masayuki Okuya[1,†]

[1] Electronics and Materials Science Course, Department of Engineering, Graduate School of Integrated Science and Technology, Shizuoka University, Hamamatsu, Japan

A porous-TiO_2 layer was formed using a non-equilibrium planar plasma under atmospheric pressure. With a planar plasma, which decayed rapidly on the electrode in air, a small amount of plasma was supplied to the titanium–peroxo complex precursor pre-coated on a substrate during film formation. However, by applying a magnetic field to the plasma, the spatial distribution was expanded to reach the bulk of the precursor layer, and the oxidation process was accelerated under a nitrogen and oxygen mixture gas flow. We found that active N–O plasma species induced under a high nitrogen gas concentration played an important role in oxidizing and crystallizing the precursor to the anatase TiO_2 phase. The precursor was employed as a binder to promote the necking process between the TiO_2 particles to form a porous layer. A dye-sensitized solar cell (DSSC) fabricated with a porous-TiO_2 layer showed a maximum conversion efficiency of 3.9 %. Although the photovoltaic performance was lower than that of a general DSSC, a practical plastic substrate is acceptable in this low-temperature film formation technique, which will be developed into a convenient tool to produce a DSSC for daily use.

©2022 The Ceramic Society of Japan. All rights reserved.

Key-words : Dielectric barrier discharge, Planar plasma, Thin film, Dye-sensitized solar cell, Titanium–peroxo complex, Titanium dioxide

[Received November 4, 2021; Accepted December 27, 2021]

1. Introduction

Global environmental problems and resource depletion have become serious issues over the last few decades. Among the many renewable and environment-friendly energy sources, the development of solar power systems is one of the key strategies to solve these problems. Although silicon solar cells generate high electric power and are in daily use, these systems are rather expensive owing to the high vacuum and high-temperature manufacturing process required to produce a pure silicon device. Dye-sensitized solar cells (DSSCs) have been studied as an alternative photovoltaic system to silicon cells because most of the fabrication process can be conducted in air with low-priced materials. Recently, DSSCs have been applied to perovskite solar cells (PSCs), which exhibits a high conversion efficiency comparable to that of silicon cells. However, PSCs contain lead compounds, which are far from environmentally friendly devices. Moreover, a PSC must be kept free from moisture, and a long-term stabilized operation is now under development.[1),2)] Tin[3),4)] and bismuth[5)–7)] are potential alternatives to lead. However, the photovoltaic performance of these elements is significantly reduced. However, conventional DSSCs have reached the stage of some practical applications, although the conversion efficiency is still lower than that of PSCs. In producing a DSSC, high-temperature sintering at 500 °C is required to form a porous-TiO_2 layer for the working electrode.[8)–10)] Owing to the high-temperature sintering process, only a heat-resistant substrate is acceptable for this photovoltaic device, which prevents the use of a practical plastic substrate in a DSSC.

Plasma technology has been widely used for surface modification,[11)–13)] water treatment,[14),15)] and manufacturing electronic devices.[16),17)] In general, a plasma that is induced under atmospheric pressure is divided into two types: a thermal equilibrium plasma represented by an arc discharge[18)–22)] and a non-equilibrium plasma represented by a dielectric barrier discharge.[23)–28)] In a thermal equilibrium plasma, both the electron and ionic temperatures maintain a balance in the closed system. On the other hand, in a non-equilibrium plasma, the electron temperature is above tens of thousands of Kelvin, whereas the ionic temperature decays rapidly to room temperature on the electrode. In addition, a non-equilibrium plasma is very convenient for supplying high energy to the selective area on a substrate without heating the entire volume, which is a useful method of direct patterning in film formation. Recently, we developed a novel plasma technology for a

† Corresponding author: M. Okuya; E-mail: tcmokuy@shizuoka.ac.jp

©2022 The Ceramic Society of Japan

This is an Open Access article distributed under the terms of the Creative Commons Attribution License (https://creativecommons.org/licenses/by-nd/4.0/), which permits unrestricted use, distribution, and reproduction in any medium, provided the original work is properly cited.

low-temperature film formation system. We have reported the film formation of ZnO by irradiating a zinc ammonium complex precursor with a non-equilibrium planar plasma induced by dielectric barrier discharge.[29] Active plasma species induced under pure oxygen gas flow promoted the hydrolysis of the precursor to be crystallized into a hexagonal ZnO phase. As the non-equilibrium plasma was induced along a metal grid on the electrode, and the substrate temperature was kept below 80 °C during film formation, a ZnO film was successfully formed on a polyethylene terephthalate substrate.

Several plasma technologies have been employed to produce DSSCs for decades. However, most of them utilize the technology for surface cleaning and/or modification of the porous-TiO_2 layer for a working electrode presintered in an electric furnace at high temperature.[30)–33)] In contrast, we have reported a plasma technology to form a porous-TiO_2 layer for a DSSC at a substrate temperature below 80 °C.[34)] However, the plasma induced under atmospheric pressure decayed rapidly, and the vertical distribution of the planar plasma on the electrode was too thin to allow annealing of a porous-TiO_2 layer to produce a high-performance DSSC. In this study, we applied a 0.17 T magnetic field perpendicular to the plasma during film formation. Under the magnetic field, a Lorentz force was induced in the system to expand the vertical distribution of the planar plasma on the electrode, and a high-energy plasma was supplied to the bulk of the porous-TiO_2 layer. Although the photovoltaic performance of the cell fabricated in this study is lower than that of a general DSSC, we found that this low-temperature film formation technique opens the way to the subsequent progress of a DSSC for eco-friendly use.

2. Experimental

A hand-made electrode for discharge was prepared as follows. A metal grid pattern was screen-printed with a resistive paste (R-2010L, Shoei Chemical Inc.) on both faces of an alumina plate, 50 × 25 × 0.6 mm^3 in size, and sintered at 1150 °C for 20 min. Then, a conductive paste (H-4566, Shoei Chemical Inc.) was screen-printed to form two terminals on the grids and sintered at 900 °C for 15 min. Finally, an insulating paste (QM44, Dupont) was screen-printed to fully cover the grid except for two terminals, and sintered at 1000 °C for 15 min to complete the electrode. The detailed procedure for preparing an electrode has been reported previously.[34)] **Figure 1**(a) shows a photograph of the discharge electrode. A blue plasma originating from nitrogen in air was induced along a "P-shape" grid by applying a sinusoidal bias of 4 kHz and 10 kV with a function generator (WF1965, NF Co.) through a high-voltage amplifier (Model 20/20 C, Trek Inc.). The energy of the plasma was estimated using a capacitor of 330 nF incorporated into the electric circuit of the discharge system.[35)] When plasma was induced on the electrode, a typical rhombic Lissajous figure was displayed on the connected digital oscilloscope (TDS2024B, Tektronix Inc.), and the area of the figure corresponds to the plasma energy.

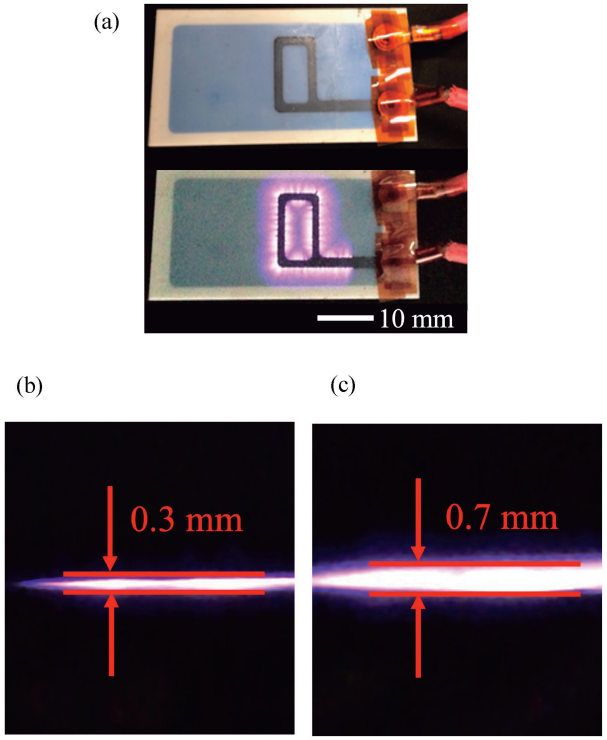

Fig. 1. Photographs of a hand-made discharge electrode; (a) the electrode (top) before and (bottom) after applying AC bias of 4 kHz and 10 kV in air, the vertical plasma distribution on the electrode (b) with no field, and (c) with applying a 0.17 T of magnetic field.

As mentioned previously, a plastic substrate is acceptable for this non-equilibrium plasma-film formation technique. However, a higher electric power is required to form a TiO_2 layer, and the hand-made electrode generates many fine sparks in discharge, which seriously damages the plastic substrate. To produce a high-performance DSSC, we employed a glass substrate (Corning 1737) in this study.

We prepared 0.1 M of di-*n*-butyltin(IV) diacetate (DBTDA, Tokyo Kasei Kogyo) ethanol solution with an additive of ammonium fluoride (NH_4F, FUJIFILM Wako Pure Chemical) with a molar ratio of [NH_4F]/[DBTDA] = 1.6, and this was sprayed by a nozzle (Lumina STA-6R-1 mmϕ, Fuso Seiki) with compressed air onto a heated glass substrate. The mist was pyrolyzed on the substrate at a substrate temperature of 500 °C to form an FTO film in air with a sheet resistance and average transmittance in the visible region of 10 Ω/sq and 80 %, respectively.[29),36)–41)] Then, 0.1 M of bis (2,4-pentanedionato) titanium(IV) oxide (Tokyo Kasei Kogyo) ethanol solution was sprayed onto the FTO-coated glass substrate at 500 °C to deposit a dense-TiO_2 buffer layer.[39)–41)] Before spraying the solution, we placed another cover glass on a portion of the FTO-coated glass to leave 5 mm of bare FTO layer for the terminal of the device. A commercial TiO_2 suspension (STS-02; Ishihara Sangyo) and powder (P25; Degussa) were mixed at a molar ratio of [STS-02]/[P25] = 1.0, to prepare a source solution for the porous-TiO_2 layer. The solution was sprayed onto the buffer layer at 150 °C in air.

Before spraying the solution, the glass was covered with a heat-resistant tape with a circular hole to deposit a porous-TiO_2 layer with an apparent area of 0.23 cm^2 on the buffer layer.[39)–41)] A reddish–yellow titanium–peroxo complex precursor was prepared from titanium(IV) tetraisopropoxide (TTIP) (Kanto Chemical) by adding 1.0 M of hydrogen peroxide (FUJIFILM Wako Pure Chemical, 30 wt %) with a molar ratio of $[TTIP]/[H_2O_2] = 0.1$ with cooling by ice water.[42),43)] Then, the porous-TiO_2 layer on the FTO-coated glass was immersed in the titanium–peroxo complex solution for 30 min. After removing the glass from the solution, the glass was dried in air and placed in the holder to face the porous-TiO_2 layer with an electrode for discharge. The distance between the porous-TiO_2 layer and the electrode was fixed at 0.1 mm using a goniometer. Neodymium magnets were set on both sides of the electrode to apply a 0.17 T magnetic field, and then a planar plasma was induced under a nitrogen and oxygen mixture gas flow of 5 L/min.[34)] Plasma irradiation of the porous-TiO_2 layer was conducted for 40 min. A two-step stacking process was conducted to form a porous-TiO_2 layer with a thickness of 10 µm. A porous-TiO_2 layer with a thickness of 1, 3, or 5 µm was formed in the first step as mentioned previously. Then, the second step was performed to form a porous-TiO_2 layer with a thickness of 9, 7, or 5 µm on the first layer using the same procedure to finally form 10-µm-thick porous layers.

The films formed from a titanium–peroxo complex precursor were characterized by X-ray diffraction (XRD; RINT Ultima III, Rigaku) with a scanning speed of 5°/min at a step of 0.03°, using Cu Kα radiation at 40 kV and 40 mA. The surface morphology of the porous-TiO_2 layer was observed using scanning electron microscopy (JSM-6335F, JEOL Ltd.). N719 (Ruthenium 535-bisTBA, FUJIFILM Wako Pure Chemical) dye was adsorbed on the surface of the porous-TiO_2 layer by soaking the layer in a 1×10^{-4} M ethanol solution at 45 °C for 18 h. Finally, a dye-adsorbed TiO_2 working electrode and a Pt counter electrode were clamped by clips, and then a drop of anhydrous I^-/I_3^- electrolyte [0.5 M of 1,2-dimethyl-3-propylimidazolium iodide (Kanto Chemical), 0.08 M of lithium iodide (FUJIFILM Wako Pure Chemical), 0.42 M of 4-tert-butylpyridine (Tokyo Kasei Kogyo), 4.2×10^{-3} M of iodine (Kanto Chemical), and 0.17 M of guanidine thiocyanate (FUJIFILM Wako Pure Chemical) in acetonitrile (FUJIFILM Wako Pure Chemical)] was injected between the two electrodes by capillary force to fabricate a DSSC.[44)–47)]

The photovoltaic performance of the cell was measured under quasi-sunlight of AM-1.5 and 100 mA/cm^2 (HAL-320, Asahi Spectra). The incident photon-to-current conversion efficiency (IPCE) was measured with a constant photon mode using an IPCE system (PVL-4000, Asahi Spectra). The electrochemical impedance was measured using an electrochemical test system (1470E and 1255B, Solartron) in the AC frequency range of 0.1 to 100 kHz. The amount of dye adsorbed on the porous-TiO_2 was evaluated by spectrophotometry (UV-1800, Shimadzu).

3. Results and discussion

Figures 1(b) and 1(c) show photographs of the vertical distribution of a plasma induced on a self-made electrode at 4 kHz and 10 kV in air before and after applying a 0.17 T magnetic field, respectively. Under a 0.17 T magnetic field, the Lorentz force was induced to discharge electrons, and an apparent vertical distribution of the plasma induced by an interaction between the electrons and atmospheric gases was enhanced from 0.3 to 0.7 mm in thickness on the electrode, which is supposed to lead to an efficient plasma treatment for film formation. The energy of the plasma induced under a nitrogen and oxygen mixture gas flow did not depend on the atmosphere and was estimated to be 3.5–4.0 J/s, indicating that active plasma species induced on the electrode remain in almost the same high-energy level long enough to decompose the titanium–peroxo complex precursor within a few seconds.

A planar plasma was irradiated onto a titanium–peroxo complex precursor pre-coated on a glass substrate to investigate the effect of plasma treatment on the oxidation and crystallization of the TiO_2 phase. **Figure 2** shows the XRD patterns of the films formed under various atmospheres. An amorphous structure was observed for the film formed under pure nitrogen and oxygen gas flow. On the other hand, under a gas mixture flow of $N_2/O_2 = 99/1$ and 99.8/0.2 in volume, the (101) peak of the anatase TiO_2 phase was observed. A titanium–peroxo complex precursor was reported to form a TiO_6 octahedral structure in solution. Oxygen ions confirm direct bonds to a titanium ion, and a face-shared linking of each octahedral TiO_6 was formed in a molecular structure, which is close to that of an anatase TiO_2 crystal structure, and then decomposes and crystallizes easily at around 300 °C.[48)–50)] However,

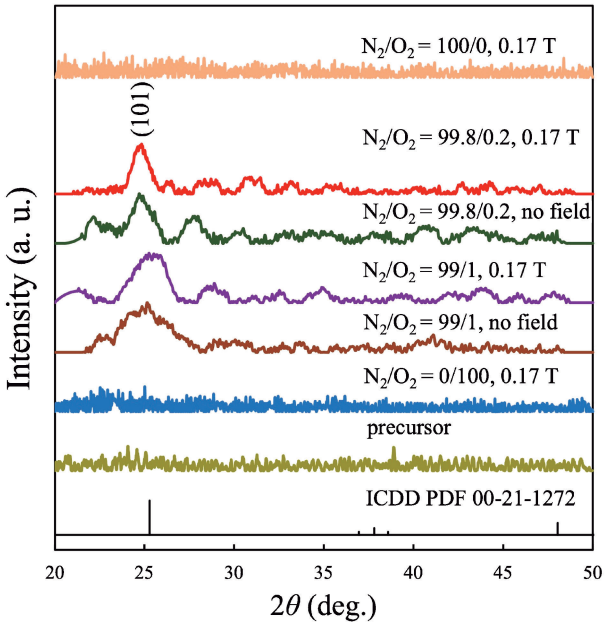

Fig. 2. XRD patterns of films formed from a titanium–peroxo precursor with irradiating a non-equilibrium planar plasma induced under various atmospheres.

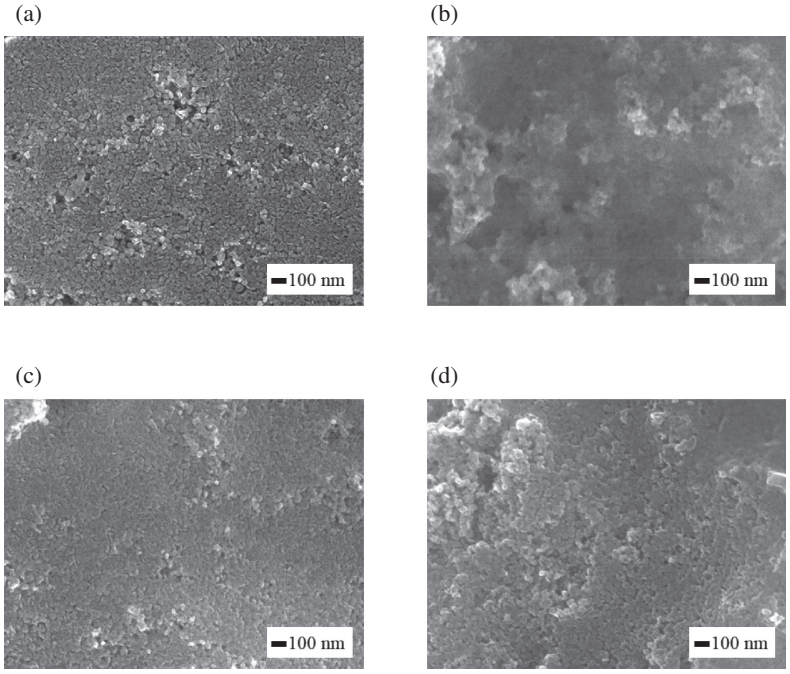

Fig. 3. Surface morphology of porous-TiO_2 layers; (a) as-deposited, (b) immersing in a titanium–peroxo precursor solution and drying in air, and plasma treatment under a gas mixture flow of $N_2/O_2 = 99.8/0.2$ with (c) no field, and (d) a 0.17 T magnetic field.

because the substrate temperature was kept below 80 °C with a cooling system during film formation, we assume that crystallization was not conducted by thermal decomposition but by a chemical reaction with active plasma species. Under the flow of a mixture of nitrogen and oxygen, various plasma species are generated, such as O, O^+, O_2, O_2^+, N, N^+, N_2, N_2^+, NO^+, and NO.[51)–53)] Suetomi et al. reported that N–O meta-stable plasma was mainly induced under a gas mixture flow of $N_2/O_2 = 99.8/0.2$.[52),53)] We suppose that N–O plasma species act as an effective oxidant to the titanium–peroxo complex, although a detailed mechanism has not yet been clarified. The crystallization of the anatase TiO_2 phase was further accelerated by applying a 0.17 T magnetic field during film formation. The grain size of the film from the half width of the (101) peak was calculated to be 7.2 and 5.9 nm with and without applying a magnetic field, respectively, indicating that more active plasma species reached the bulk of the precursor because of the vertical expansion on the electrode under a magnetic field.

Figure 3 shows the surface morphology of the porous-TiO_2 layers formed under a gas mixture flow of $N_2/O_2 = 99.8/0.2$. The as-deposited layer exhibited a porous structure with a particle size of 13 nm, as shown in Fig. 3(a). However, the layer exhibited low adhesion and easily detached from the substrate. After immersing the layer in the precursor solution and drying in air, the pores were fully packed with the precursor, as shown in Fig. 3(b). The mechanical strength of the layer increased significantly after the plasma treatment, and a porous structure was observed again, as shown in Figs. 3(c) and 3(d), indicating that the precursor in the pores crystallized to an anatase TiO_2 phase during plasma treatment and enhanced the necking process between TiO_2 particles to form a porous-TiO_2 layer. The amount of N719 dye loading on the surface of the porous-TiO_2 layer was estimated as 1.93×10^{-7} and 1.56×10^{-7} mol/cm^2 for the layer formed with and without applying the 0.17 T magnetic field, respectively. The amount is assumed to be comparable within the resolution of the measurement system, and the specific surface area of these layers was estimated to be approximately 50 m^2/g, which is a typical value of a general DSSC.[54)–56)]

DSSCs were fabricated with a porous-TiO_2 layer, and the photovoltaic parameters are summarized in **Table 1**. Before the plasma treatment, the mechanical strength between the TiO_2 particles within the porous layer was too weak to exhibit adequate photovoltaic parameters. This is due to the high internal electric resistance, which causes the frequent recombination of photoelectrons. Then, well-crystallized bonding between TiO_2 particles should be produced for the porous-TiO_2 layer. In a general DSSC, a 10-μm-thick TiO_2 layer is required for high photovoltaic performance. However, a 10-μm-thick layer formed by this plasma technique revealed a low short-circuit current density (Jsc) of 1.2 mA/cm^2, leading to a conversion efficiency (η) of less than 1 %. This is because the planar plasma decays exponentially in the vertical distribution on the electrode under atmospheric pressure, and an effective plasma treatment was not conducted on the bulk of the porous-TiO_2 layer, which resulted in high internal resistance within the cell. To solve this problem, we employed a two-step plasma treatment to form double-layered TiO_2. The thicknesses of the first and second porous-TiO_2 layer

Table 1. Photovoltaic parameters and the real part of four arcs in impedance spectra of DSSCs fabricated with a porous-TiO_2 layer prepared by a two-step stacking process. The thickness of the first and second porous-TiO_2 layer are abbreviated as (1st + 2nd)

TiO_2 thickness (μm)	Magnetic field (T)	*J*sc (mA/cm^2)	*V*oc (V)	*FF*	*η* (%)	R_0 (Ω)	R_1 (Ω)	R_2 (Ω)	R_3 (Ω)	R_4 (Ω)
TTIP immersing										
10+0	—	0.52	0.82	0.48	0.21	N/A	N/A	N/A	N/A	N/A
Plasma treatment										
10+0	—	1.2	0.79	0.63	0.59	13	60	740	900	140
	0.17	2.9	0.81	0.73	1.7	6	30	240	380	60
1+9	—	4.3	0.78	0.70	2.4	20	22	124	254	50
	0.17	5.5	0.74	0.66	2.7	15	12	86	250	60
3+7	—	6.6	0.76	0.68	3.4	8	20	80	182	40
	0.17	7.0	0.77	0.72	3.9	16	16	30	120	46
5+5	—	5.7	0.76	0.67	2.9	9	24	96	244	56
	0.17	6.6	0.75	0.68	3.4	14	16	70	156	44
Electric furnace	Temperature (°C)									
10+0	300	6.7	0.75	0.72	3.6	19	26	36	142	32
	500	15.8	0.71	0.68	7.6	17	7	12	102	6

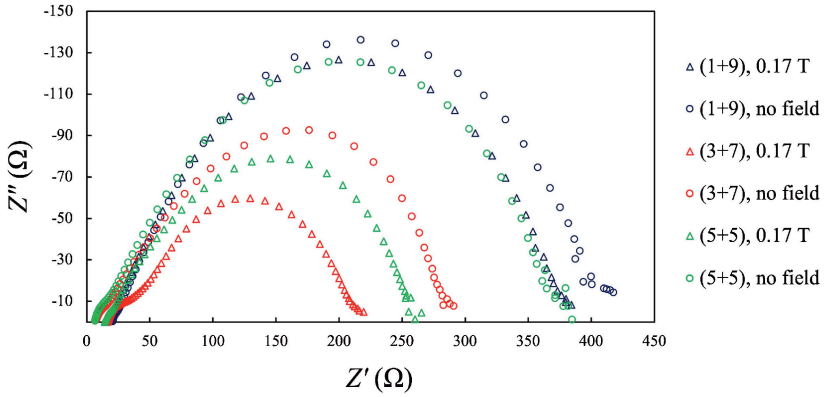

Fig. 4. Nyquist plot of impedance spectra of DSSCs fabricated with various configurations of porous-TiO_2 layers formed with a plasma induced under a gas mixture flow of $N_2/O_2 = 99.8/0.2$. The thickness of the first and second porous-TiO_2 layer are abbreviated as (1st + 2nd).

are abbreviated as (1st + 2nd) hereafter. The cell with the porous-TiO_2 layer of (3 + 7) μm exhibited the highest *J*sc of 6.6 mA/cm^2, and the conversion efficiency reached as high as 3.4 %. On the other hand, the open-circuit voltage (*V*oc) and fill factor (*FF*) did not depend on the configuration of the porous-TiO_2 layer and showed almost constant values in all cells. We found that the two-step plasma treatment is a useful way to form a porous-TiO_2 layer that enhances *J*sc. To check the details of carrier transportation within the cell, electrochemical impedance measurements were conducted. **Figure 4** shows the Nyquist plots of the impedance measurements of the DSSCs. The spectra displayed in the figure were estimated using *Z*-view plot software installed in the measurement system according to the equivalent electric circuit.[57] Each spectrum consisted of a series resistance, R_0, and four arcs, ω_1–ω_4. The series resistance, R_0, and real parts of four arcs, R_1–R_4, are summarized in Table 1. The sum of the resistances of the FTO and buffer-TiO_2 layer,[47] R_0, did not depend on the configuration of the porous-TiO_2 layer, and showed almost a constant value of approximately 20–24 Ω. The resistance R_1 corresponds to the interface resistance at the FTO/buffer-TiO_2/porous-TiO_2 or Pt counter electrode/electrolyte. In this study, because the charge transportation at the Pt counter electrode/electrolyte is not related to the porous-TiO_2 layer, we can treat R_1 as the interface resistance at FTO/buffer-TiO_2/porous-TiO_2, although a constant contribution from Pt counter electrode/electrolyte should be considered. The cell with the porous-TiO_2 layer of (3 + 7) μm showed the smallest R_1 of 20 Ω, indicating that the plasma effectively reached the bulk of the porous-TiO_2/FTO interface to improve the adhesion between the layers, accelerating efficient photoelectron transport within the cell. However, the effect of the plasma treatment declined with other porous configurations. In the porous layer of (1 + 9) μm, the first layer was too thin, and the influence of high-energy plasma etching was not negligible, leading to a coarse layer with a lower adhesion to the FTO layer. On the other hand, in the porous layer of (5 + 5) μm, the first layer was too thick for the plasma to fully reach the bulk of the TiO_2/FTO interface. The resistance R_2, the interparticle resistance within a porous-TiO_2 layer, and R_3, the interface resistance at porous-TiO_2/dye/electrolyte, is high for the cell with a layer of (1 + 9) μm, indicating a lower crystallized bonding between TiO_2 particles. This is because the second layer was too thick

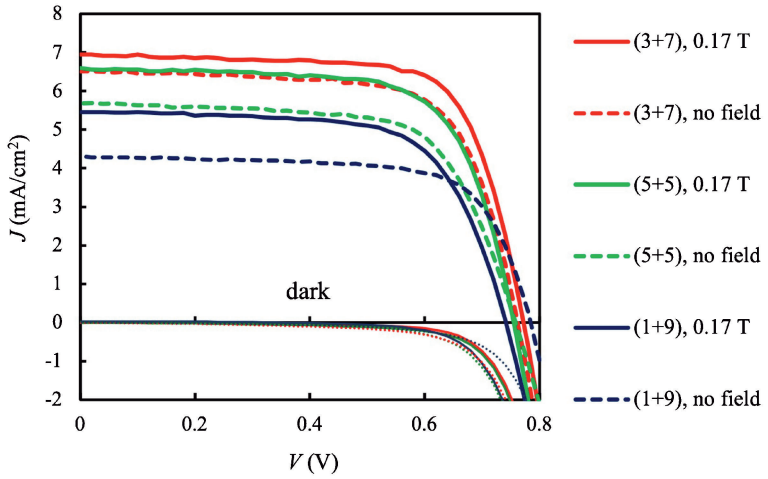

Fig. 5. *J-V* curves of DSSCs fabricated with various configurations of porous-TiO_2 layers formed with a plasma induced under a gas mixture flow of $N_2/O_2 = 99.8/0.2$. The thickness of the first and second porous-TiO_2 layer are abbreviated as (1st + 2nd).

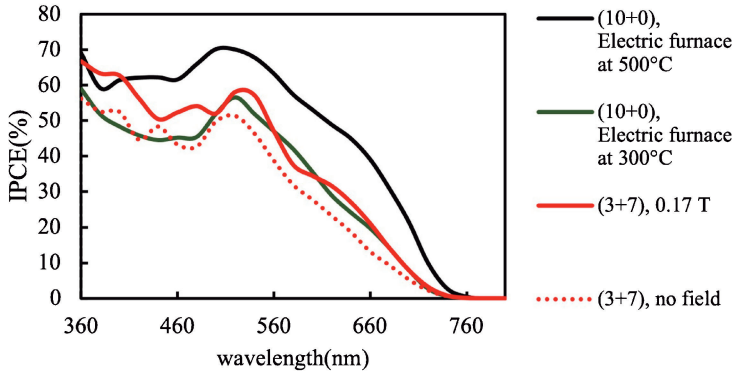

Fig. 6. IPCE spectra of DSSCs fabricated with the porous-TiO_2 layers formed with a plasma induced under a gas mixture flow of $N_2/O_2 = 99.8/0.2$ with and without applying a 0.17 T magnetic field. The thickness of the first and second porous-TiO_2 layer are abbreviated as (1st + 2nd). The spectra of general cells produced at 300 and 500 °C in an electric furnace in air are shown as references.

for an effective plasma treatment, and some weak necking region was left in the bulk of the second layer. In addition, the interface resistance between the first and second layer seems to contribute to some extent and cannot be negligible. The resistance, R_4, of ionic diffusion in the electrolyte did not depend on the configuration of the porous-TiO_2 layer. This is because the ionic diffusion process is not related to the porous layer. We concluded that the interfacial resistance at FTO/porous-TiO_2 was reduced for the first layer with a thickness of 3 µm and that the subsequent plasma treatment to the second layer was effectively applied to the bulk to prepare an ideal working electrode. However, the conversion efficiency of these cells was much lower than that of a general DSSC. This is because the internal resistance is still high and causes frequent recombination within the cell, compared with that of a general DSSC produced at 500 °C in a conventional electric furnace. We suppose that the plasma treatment was not sufficient to complete the necking process within the porous-TiO_2 layer during plasma irradiation. To enhance the photovoltaic performance, a 0.17 T magnetic field was applied to induce a Lorentz force for a vertical expansion of the plasma distribution on the electrode for an effective plasma treatment to the bulk of the porous-TiO_2 layer. **Figure 5** shows the *J–V* curves of DSSCs fabricated with various porous-TiO_2 layers. A typical rectification curve for a photovoltaic device was observed for all the cells in the dark. The photovoltaic performance was improved for the cell formed with an applied magnetic field. In particular, the interface resistances R_2 and R_3 were significantly reduced by the application of a magnetic field. The effect of the magnetic field appears to be remarkable with increasing thickness of the second porous-TiO_2 layer. In particular, for the cell with a porous-TiO_2 layer of (3 + 7) µm, the conversion efficiency reached a maximum value of 3.9 %, which was attributed to the reduction of R_2 and R_3. **Figure 6** shows the IPCE spectra of DSSCs fabricated with the porous-TiO_2 layer formed with and without applying a magnetic field. With applying a magnetic field during film formation, the spectrum was enhanced at all wavelengths, although the amount of the dye loading on the porous-TiO_2 layer is comparable in both cells. Since

the IPCE spectrum directly reflects photoelectrons, we found that the amount of the dye loading on the porous-TiO_2 layer is not the only parameter that governs *J*sc and that the internal resistance within the cell is the main parameter in this case. However, the photovoltaic performance was much lower than that of a general cell, and was comparable to that produced at 300 °C in a conventional electric furnace in air. Further optimization of the 3D handling of plasma is required to form an ideal porous-TiO_2 layer for a DSSC. Although the photovoltaic performance remains lower than that of a general DSSC, the substrate temperature was maintained below 80 °C during film formation. We suppose that this plasma technology is a convenient tool for producing a DSSC on a light and flexible plastic substrate. Further optimization of the plasma technology for effective film formation is required for the next step.

4. Summary

In this study, we developed a non-equilibrium atmospheric planar plasma into a film formation technique to form a porous-TiO_2 layer for a DSSC. The titanium–peroxo complex precursor was oxidized and crystallized into an anatase TiO_2 phase during the plasma treatment. Using this characteristic, we employed the precursor as a necking agent between the TiO_2 particles to form a porous-TiO_2 layer. We found that N–O active plasma species played an important role in forming a well-crystallized bonding between TiO_2 particles to form a porous-TiO_2 layer, although the detailed mechanism of film formation has not yet been clarified. A two-step plasma treatment was conducted to reduce the internal resistance within the porous-TiO_2 layer for a DSSC. The interface resistance within the cell was reduced by applying a magnetic field to the plasma, which was attributed to an effective spatial expansion of the plasma to reach the bulk of the porous layer during film formation. At this moment, the photovoltaic performance is lower than that of a general DSSC; however, the possibility of fabricating DSSCs on plastic substrates using a non-equilibrium plasma has been demonstrated here.

Acknowledgment This work was supported by JSPS KAKENHI Grant Number JP20K03916.

References

1) H.-S. Kim, J.-Y. Seo and N.-G. Park, *ChemSusChem*, 9, 2528–2540 (2016).
2) J. Zhang, G. Hodes, Z. Jin and S. Liu, *Angew. Chem. Int. Edit.*, 58, 15596–15618 (2019).
3) S. Shao, J. Liu, G. Portale, H.-H. Fang, G. R. Blake, G. H. ten Brink, L. J. A. Koster and M. A. Loi, *Adv. Energy Mater.*, 8, 1702019 (2018).
4) T.-B. Song, T. Yokoyama, S. Aramaki and M. G. Kanatzidis, *ACS Energy Lett.*, 2, 897–903 (2017).
5) I. Turkevych, S. Kazaoui, E. Ito, T. Urano, K. Yamada, H. Tomiyasu, H. Yamagishi, M. Kondo and S. Aramaki, *ChemSusChem*, 10, 3754–3759 (2017).
6) M. S. Shadabroo, H. Abdizadeh, M. Shabani and M. R. Golobostanfard, *Inorg. Chem.*, 60, 11110–11119 (2021).
7) G.-X. Liang, X.-Y. Chen, Z.-H. Chen, H.-B. Lan, Z.-H. Zheng, P. Fan, X.-Q. Tian, J.-Y. Duan, Y.-D. Wei and Z.-H. Su, *J. Phys. Chem. C*, 123, 27423–27428 (2019).
8) G. Wang, W. Xiao and J. Yu, *Energy*, 86, 196–203 (2015).
9) S. V. Umale, S. N. Tambat, V. Sudhakar, S. M. Sontakke and K. Krishnamoorthy, *Adv. Powder Technol.*, 28, 2859–2864 (2017).
10) X. Liu, C. Zhang, S. Liu and Y. Xiong, *Optik*, 160, 277–282 (2018).
11) V. Multanen, G. Chaniel, R. Grynyov, R. Y. Loew, N. K. Siany and E. Bormashenko, *Colloid. Surface. A*, 461, 225–230 (2014).
12) M. L. Steen, A. C. Jordan and E. R. Fisher, *J. Membrane Sci.*, 204, 341–357 (2002).
13) S. M. Pelagade, N. L. Singh, A. Qureshi, R. S. Rane, S. Mukherjee, U. P. Deshpande, V. Ganesan and T. Shripathi, *Nucl. Instrum. Meth. B*, 289, 34–38 (2012).
14) S. Kanazawa, S. Geng, T. Okawa, S. Akamine and R. Ichiki, *Int. J. Plasma Environ. Sci. Technol.*, 7, 21–25 (2013).
15) K. Takahashi and K. Takaki, *Vac. Surf. Sci.*, 61, 131–142 (2018) [in Japanese].
16) S. Samukawa, V. M. Donnelly and M. V. Malyshev, *Jpn. J. Appl. Phys.*, 39, 1583–1596 (2000).
17) K. Ono, H. Ohta and K. Eriguchi, *Thin Solid Films*, 518, 3461–3468 (2010).
18) P. Zhao, G. Ni, Y. Jiang, L. Chen, M. Chen and Y. Meng, *J. Hazard. Mater.*, 181, 580–585 (2010).
19) C. Wang, H. Cui, Z. Zhang, W. Xia and W. Xia, *Contrib. Plasm. Phys.*, 57, 395–403 (2017).
20) A. V. Samokhin, N. V. Alekseev, S. A. Kornev, M. A. Sinaiskii, Y. V. Blagoveschenskiy and A. V. Kolesnikov, *Plasma Chem. Plasma P.*, 33, 605–616 (2013).
21) P. V. Krasovskii, A. V. Samokhin, A. A. Fadeev and N. V. Alexeev, *Adv. Powder Technol.*, 27, 1669–1676 (2016).
22) S. Samal, *J. Clean. Prod.*, 142, 3131–3150 (2017).
23) Y. Setsuhara, *Arch. Biochem. Biophys.*, 605, 3–10 (2016).
24) Z. Fang, Y. Qiu and E. Kuffel, *IEEJ Trans. FM*, 127, 519–523 (2007).
25) J. Miyamoto, T. Inoue, K. Tokuno, H. Tsutamori and P. Abraha, *Tribol. Online*, 11, 460–465 (2016).
26) S. Dahle, R. Gustus, W. Viöl and W. Maus-Friedrichs, *Plasma Chem. Plasma P.*, 32, 1109–1125 (2012).
27) Y. Xu, Y. Zhang, L. Li, K. Ding, Y. Guo, J. Shi, X. Huang and J. Zhang, *Plasma Chem. Plasma P.*, 39, 937–947 (2019).
28) A. Yehia, A. Mizuno and M. A. M. El-Osealy, *Jpn. J. Appl. Phys.*, 43, 5558–5561 (2004).
29) M. Okuya, K. Nabeta, Y. Shibayama, S. Kanezashi, M. Tan, M. Iyoda, M. Shikatani, Y. Sonohara and I. Yagi, *Appl. Phys. Express*, 7, 015501 (2014).
30) S. Zen, Y. Teramoto, R. Ono and T. Oda, *J. Appl. Phys.*, 51, 056201 (2012).
31) H. J. Kim, J. Kim and B. Hong, *Appl. Surf. Sci.*, 274, 171–175 (2013).
32) J. T. Kim and S. H. Kim, *Sol. Energ. Mat. Sol. C.*, 95, 336–339 (2011).
33) G. D. Rajmohan, X. J. Dai, T. Tsuzuki, P. R. Lamb, J. du Plessis, F. Huang and Y.-B. Cheng, *Thin Solid Films*,

545, 521–526 (2013).
34) M. Okuya, S. Mayumi, R. Okumura, Y. Masuda and I. Yagi, *Jpn. J. Appl. Phys.*, 60, 045501 (2021).
35) H. E. Wagner, R. Brandenburg, K. V. Kozlov, A. Sonnenfeld, P. Michel and J. F. Behnke, *Vacuum*, 71, 417–436 (2003).
36) M. Okuya, S. Kaneko, K. Hiroshima, I. Yagi and K. Murakami, *J. Eur. Ceram. Soc.*, 21, 2099–2102 (2001).
37) M. Okuya, K. Nakade and S. Kaneko, *Sol. Energ. Mat. Sol. C.*, 70, 425–435 (2002).
38) M. Okuya, D. Osa and S. Kaneko, *Key Eng. Mat.*, 247, 228–229 (2002).
39) M. Okuya, K. Nakade, D. Osa, T. Nakano, G. R. A. Kumara and S. Kaneko, *J. Photoch. Photobio. A*, 164, 167–172 (2004).
40) M. Okuya, K. Shiozaki, N. Horikawa, T. Kosugi, G. R. A. Kumara, J. Madarász, S. Kaneko and G. Pokol, *Solid State Ionics*, 172, 527–531 (2004).
41) M. Okuya, K. Ohashi, T. Yamamoto and J. Madarász, *Electrochemistry*, 76, 132–135 (2008).
42) S. I. Seok, B. Y. Ahn, N. C. Pramanik and H. Kim, *J. Am. Ceram. Soc.*, 89, 1147–1149 (2006).
43) M. Hočevar, U. O. Krašovec and M. Topič, *J. Sol-Gel Sci. Techn.*, 68, 67–74 (2013).
44) T. Yamamoto, K. Ohashi and M. Okuya, *Trans. Mater. Res. Soc. Jpn.*, 35, 409–412 (2010).
45) G. R. A. Kumara, C. S. K. Ranasinghe, E. N. Jayaweera, H. M. N. Bandara, M. Okuya and R. M. G. Rajapakse, *J. Phys. Chem. C*, 118, 16479–16485 (2014).
46) R. Otsuka, T. Endo, T. Takano, S. Takemura, R. Murakami, R. Muramoto, J. Madarász and M. Okuya, *Jpn. J. Appl. Phys.*, 54, 08KF03 (2015).
47) M. Okuya, J. Sato, T. Endo, R. Iwaki, S. Takemura, R. Muramoto, V. Nagygyörgy, J. Madarász, S. Nakao, N. Yamada, E. Sakai, T. Hitosugi and T. Hasegawa, *J. Am. Ceram. Soc.*, 101, 5071–5079 (2018).
48) M. Nag, S. Ghosh, R. K. Rana and S. V. Manorama, *J. Phys. Chem. Lett.*, 1, 2881–2885 (2010).
49) R. S. Sonawane and S. Ramakrishna, *Mat. Sci. Eng. B-Solid*, 177, 652–660 (2012).
50) Y. Gao, Y. Masuda, W.-S. Seo, H. Ohta and K. Koumoto, *Ceram. Int.*, 30, 1365–1368 (2004).
51) K. H. Becker, U. Kogelschatz, K. H. Schoenbach and R. J. Barker, "Non-Equilibrium Air Plasmas at Atmospheric Pressure", Institute of Physics Publishing, Bristol (2005) p. 168.
52) E. Suetomi, T. Mizukoshi, K. Fukazawa and A. Saito, *Konica Minolta IEEJ Trans. FM*, 127, 423–427 (2007).
53) E. Suetomi, T. Mizukoshi, K. Fukazawa and A. Saito, *Konica Minolta Technology Report*, 3, 80–83 (2006) [in Japanese].
54) C. Li, Y. Luo, X. Guo, D. Li, J. Mi, L. Sø, P. Hald, Q. Meng and B. B. Iversen, *J. Solid State Chem.*, 196, 504–510 (2012).
55) J. Archana, M. Navaneethan and Y. Hayakawa, *J. Power Sources*, 242, 803–810 (2013).
56) M. Asemi, A. Suddar and M. Ghanaatshoar, *J. Mater. Sci.-Mater. El.*, 28, 15233–15238 (2017).
57) T. Hoshikawa, M. Yamada, R. Kikuchi and K. Eguchi, *J. Electrochem. Soc.*, 152, E68 (2005).